Publication Year	2016
Acceptance in OA@INAF	2020-05-25T09:54:58Z
Title	Variability, polarimetry, and timing properties of single pulses from PSR J1713+0747 using the large European array for pulsars
Authors	Liu, K.; Bassa, C.G.; Janssen, G.H.; Karuppusamy, R.; McKee, J.; et al.
DOI	10.1093/mnras/stw2223
Handle	http://hdl.handle.net/20.500.12386/25121
Journal	MONTHLY NOTICES OF THE ROYAL ASTRONOMICAL SOCIETY
Number	463

Monthly Notices
of the
ROYAL ASTRONOMICAL SOCIETY

MNRAS **463,** 3239–3248 (2016)
Advance Access publication 2016 September 5

doi:10.1093/mnras/stw2223

Variability, polarimetry, and timing properties of single pulses from PSR J1713+0747 using the Large European Array for Pulsars

K. Liu,[1,2]★ C. G. Bassa,[3] G. H. Janssen,[3] R. Karuppusamy,[1] J. McKee,[4] M. Kramer,[1,4] K. J. Lee,[5] D. Perrodin,[6] M. Purver,[4] S. Sanidas,[7,3] R. Smits,[3] B. W. Stappers,[4] P. Weltevrede[4] and W. W. Zhu[1]

[1]*Max-Planck-Institut für Radioastronomie, Auf dem Hügel 69, D-53121 Bonn, Germany*
[2]*Station de radioastronomie de Nançay, Observatoire de Paris, CNRS/INSU, F-18330 Nançay, France*
[3]*ASTRON, the Netherlands Institute for Radio Astronomy, Postbus 2, NL-7990 AA, Dwingeloo, the Netherlands*
[4]*Jodrell Bank Centre for Astrophysics, School of Physics and Astronomy, The University of Manchester, Manchester, M13 9PL, UK*
[5]*KIAA, Peking University, Beijing 100871, P.R. China*
[6]*INAF - Osservatorio Astronomico di Cagliari, Via della Scienza 5, I-09047 Selargius (CA), Italy*
[7]*Anton Pannekoek Institute for Astronomy, University of Amsterdam, Science Park 904, NL-1098 XH Amsterdam, the Netherlands*

Accepted 2016 September 1. Received 2016 September 1; in original form 2016 June 16

ABSTRACT

Single pulses preserve information about the pulsar radio emission and propagation in the pulsar magnetosphere, and understanding the behaviour of their variability is essential for estimating the fundamental limit on the achievable pulsar timing precision. Here we report the findings of our analysis of single pulses from PSR J1713+0747 with data collected by the Large European Array for Pulsars (LEAP). We present statistical studies of the pulse properties that include distributions of their energy, phase and width. Two modes of systematic sub-pulse drifting have been detected, with a periodicity of seven and three pulse periods. The two modes appear at different ranges of pulse longitude but overlap under the main peak of the integrated profile. No evidence for pulse micro-structure is seen with a time resolution down to 140 ns. In addition, we show that the fractional polarization of single pulses increases with their pulse peak flux density. By mapping the probability density of linear polarization position angle with pulse longitude, we reveal the existence of two orthogonal polarization modes. Finally, we find that the resulting phase jitter of integrated profiles caused by single pulse variability can be described by a Gaussian probability distribution only when at least 100 pulses are used for integration. Pulses of different flux densities and widths contribute approximately equally to the phase jitter, and no improvement on timing precision is achieved by using a sub-set of pulses with a specific range of flux density or width.

Key words: methods: data analysis – pulsars: individual: PSR J1713+0747.

1 INTRODUCTION

Millisecond pulsars (MSPs) that were spun up in accreting binary systems to reach rotational periods $\lesssim$30 ms (Alpar et al. 1982) are noted for their highly precise timing behaviour (e.g. Arzoumanian et al. 2015; Desvignes et al. 2016; Reardon et al. 2016). Their short and stable rotational period make them excellent tools for probing tiny spacetime perturbations and performing gravity experiments, including tests of General Relativity with great precision (e.g. Kramer et al. 2006; Weisberg, Nice & Taylor 2010), stringent constraints on alternative theories of gravity (e.g. Freire et al. 2012; Antoniadis et al. 2013), probes of neutron star equations-of-state (e.g. Demorest et al. 2010; Özel et al. 2010), and the ongoing search for gravitational waves in the nanohertz regime (e.g. Lentati et al. 2015; Shannon et al. 2015; Arzoumanian et al. 2016).

The success of the aforementioned timing experiments is attributed to both the regular rotation of the pulsars, and their stable integrated pulse profiles formed by averaging over tens of thousands of periods. Nevertheless, it has been known since the discovery of pulsars that the pulsed emission from every single rotation (thus single pulses) of a pulsar is highly variable. This was first noticed in canonical pulsars and more recently in MSPs (e.g. Jenet et al. 1998; Shannon & Cordes 2012; Liu et al. 2015). A consequence of such variability is the so-called pulse phase jitter phenomenon in integrated profiles, which for a given integration time places

★ E-mail: kliu@mpifr-bonn.mpg.de

© 2016 The Authors
Published by Oxford University Press on behalf of the Royal Astronomical Society

Downloaded from http://mnras.oxfordjournals.org/ at INAF Cagliari (Osservatorio Astronomico di Cagliari) on November 10, 2016

a fundamental limit on the achievable timing precision on short time-scales. Timing precision has already reached the jitter-limited regime for a few MSPs (Liu et al. 2012; Shannon & Cordes 2012), and this limit is expected to be reached for many more when the next generation of radio telescopes (e.g. the Square Kilometre Array) come online (Liu et al. 2011; Janssen et al. 2015). Most recent timing analysis has started to take into account the effect of phase jitter when modelling the noise in the timing data (e.g. Lentati & Shannon 2015; Zhu et al. 2015; Caballero et al. 2016). Detailed studies of single pulse variability in MSPs are crucial for building a comprehensive understanding of this phenomenon, if we are to push beyond this limitation. Such investigations will also provide input for the efforts to either model or mitigate jitter noise in timing data (Osłowski et al. 2011; Imgrund et al. 2015).

The origin of pulsar radio emission is associated with plasma processes in the highly magnetized pulsar magnetosphere (e.g. Cheng & Ruderman 1977; Cordes 1979; Cairns, Johnston & Das 2004), the understanding of which has still been elusive. Single pulse data preserve information of the intensity, polarization, and even waveform (if dual-polarization Nyquist sampled time series are recorded) of the emission from every single rotation. Studying single pulses can shed light on the nature of the pulsar emission mechanism, by, for example, revealing the fundamental units of coherent radiation (Cordes 1976; Gil 1985; Jenet, Anderson & Prince 2001), distinguishing different modes of polarized emission (Gil & Lyne 1995; Edwards & Stappers 2004), characterizing the temporal variability in pulse intensity (Ruderman & Sutherland 1975; Gil, Melikidze & Geppert 2003; Weltevrede, Edwards & Stappers 2006b), and so forth. Studying pulsars that display the drifting sub-pulse phenomenon can also assist in determining the viewing geometry and provide insight into the structure of the emission region (Drake & Craft 1968; Ruderman & Sutherland 1975; Rankin 1986; Qiao et al. 2004). The vast majority of single pulse emission studies has been mostly of canonical (normal, non-recycled) pulsars (see Lyne & Graham-Smith 2006, for an overview). Extending this work to include MSPs will establish a bridge between the understanding of emission physics in canonical pulsars and that in MSPs, so as to see if a common theory or model of pulsar radio emission can be applied.

A small fraction of MSPs emit occasional giant radio pulses, which have been studied in detail (Cognard et al. 1996; Knight et al. 2006; Knight 2007; Zhuravlev et al. 2013; Bilous et al. 2015). However, investigations into ordinary single pulses of MSPs have been carried out only for a limited number of bright sources (Jenet et al. 1998; Edwards & Stappers 2003; Bilous 2012; Shannon & Cordes 2012; Osłowski et al. 2014; Shannon et al. 2014; Liu et al. 2015), one of which is PSR J1713+0747. This pulsar is one of the most precisely timed pulsars and has been included in current pulsar timing array campaigns to detect gravitational waves in the nanohertz frequency range (Verbiest et al. 2016). The binary system it inhabits is also an ideal test laboratory for alternative theories of gravity (Zhu et al. 2015). Edwards & Stappers (2003) showed that there is clear modulation in the pulses from PSR J1713+0747 and that it varies across the pulse profile and as a function of observing frequency. In the fluctuation spectra, they showed that the pulsar exhibited two broad maxima corresponding to fluctuations at 0.17 and 0.35 cycles-per-period (cpp). However, the longitude dependence and a correlation with drifting sub-pulses could not be established due to the lack of sensitivity. Shannon & Cordes (2012) have shown that single pulses from PSR J1713+0747 are highly variable in phase, which already limits its timing precision with the current observing sensitivity. Thus, understanding single pulse variability of this pulsar in order to potentially mitigate its contribution to the timing noise is clearly necessary and will be the focus of this work.

The rest of this paper is structured as follows. In Section 2, we provide the details of the observation and preprocessing of the data. Section 3 presents the results from our data analysis on single pulse variability, polarization and timing properties. We conclude in Section 4 with a brief discussion and prospects for future work.

2 OBSERVATIONS

Investigations of single pulses from MSPs have been greatly restricted by their comparatively low flux density in the radio band, as well as the lack of availability of single pulse data. This is because of the large data volumes and precision timing typically being performed on integrated pulse data. The Large European Array for Pulsars (LEAP) performs monthly simultaneous observations at 1.4 GHz of 23 MSPs with the five 100-m class radio telescopes in Europe (Bassa et al. 2016). Coherently combining the voltage data from the radio telescopes delivers the sensitivity equivalent to a single dish with diameter up to 195 m and gain up to 5.7 K Jy^{-1}. For all pulsars observed, the product of coherently added voltages can be used to generate single pulse data with full polarization information and variable time resolution. In addition to LEAP's high sensitivity, the monthly observing campaign increases the chances of achieving a high signal-to-noise ratio (S/N) detection, especially for low-DM pulsars, whose flux density varies dramatically due to diffractive interstellar scintillation. Therefore, LEAP provides a data base which is ideal for single pulse studies of MSPs.

For the study in this paper, we selected 15 min of archived data obtained on MJD 56193 (23 September 2012) when a bright scintle was caught in the LEAP frequency band. The observation was conducted simultaneously with the Effelsberg Radio Telescope, the Nançay Radio telescope, and the Westerbork Synthesis Radio Telescope (WSRT).[1] At Effelsberg, the PSRIX pulsar backend was used in baseband mode to record 8 × 16 MHz bands of two orthogonal polarizations at the Nyquist rate and with 8-bit sampling (Lazarus et al. 2016). The eight bands are centred at 1340, 1356, 1372, 1388, 1404, 1420, 1436, and 1452 MHz. At Nançay, we used the NUPPI instrument (Desvignes et al. 2011) to record baseband data from four of the eight bands (1388, 1404, 1420, 1436 MHz) with an identical setup. At the WSRT, the PuMa-II system (Karuppusamy, Stappers & van Straten 2008) was used to record 8-bit baseband data of 8 × 20 MHz bands, with central frequencies at 1342, 1358, 1374, 1390, 1406, 1422, 1438 and 1454 MHz.[2] At both Effelsberg and the WSRT, the data were later copied to discs and shipped to the Jodrell Bank Observatory (JBO), where they were installed into the LEAP central storage cluster. The data from Nançay were directly transferred to JBO via internet. A full description of the LEAP observational setup can be found in Bassa et al. (2016).

Preprocessing of the data was then carried out on the CPU cluster at JBO using a software correlator developed specifically for LEAP (Smits et al., 2016). Each observation was divided into 3-min sub-integrations for correlation purposes. To calibrate the polarization of the voltage data from each individual telescope, we first dedispersed and folded the data to form an integrated profile from the entire observation. Using the polarization profile of

[1] The Lovell Telescope at Jodrell Bank was under maintenance during the observation.

[2] The WSRT bands overlap by 4 MHz, so the coherent addition later used 16 MHz out of the 20 MHz.

Downloaded from http://mnras.oxfordjournals.org/ at INAF Cagliari (Osservatorio Astronomico di Cagliari) on November 10, 2016

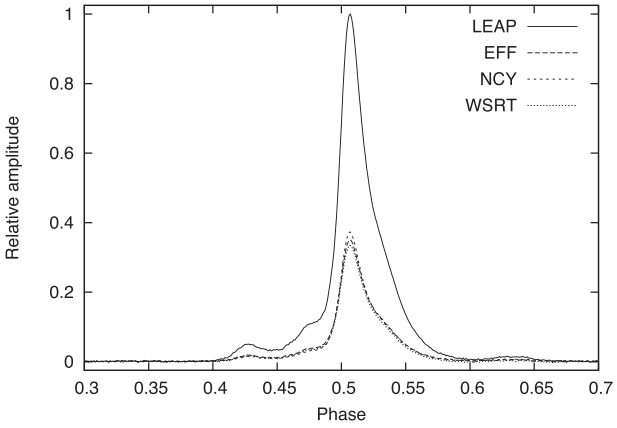

Figure 1. Total intensity profile of PSR J1713+0747 on MJD 56193 from LEAP data integrated over the entire 15-min observation, compared with those from single-telescope data. The amplitude of the profiles from individual telescopes are relative to that of the LEAP profile. The peak S/N are 896, 314, 333, 300 for LEAP, Effelsberg (EFF), Nançay (NCY), and Westerbork (WSRT), respectively, which corresponds to an addition with a 95 per cent coherency. The peak of the LEAP profile locates at phase 0.507.

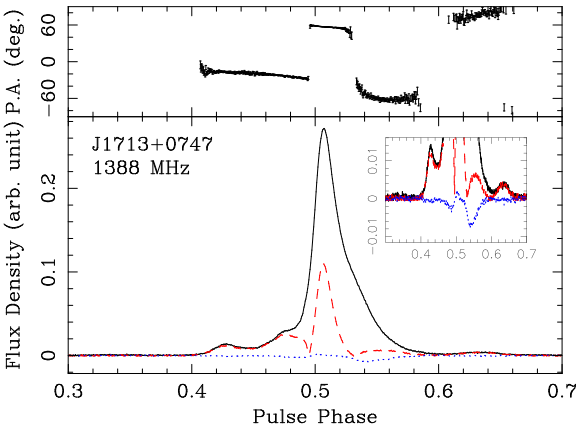

Figure 2. Polarization profile and linear polarization P.A. of PSR J1713+0747. In the lower panel, the solid (black), dashed (red) and dotted (blue) lines represent the total intensity (*I*), linear (*L*) and circular (*V*) components, respectively. The inner panel shows an enlarged view of the polarization profile. The time resolution used is 2.3 μs.

PSR J1713+0747 (from Stairs, Thorsett & Camilo 1999) obtained from the European Pulsar Network (EPN) data base,[3] we applied a template matching technique to the observed profile in order to measure the receiver properties, assuming the full reception model as in van Straten (2004). The corresponding Jones matrices were then calculated and used to calibrate the voltage data. In order to correct for the difference in voltage phase response between different backends, we used the observation of the phase calibrator J1719+0817 (performed immediately before the pulsar observation) to measure the phase offsets across the entire band, and then applied them to the data of PSR J1713+0747. As it was a very bright observation of the pulsar, we used the pulsar data itself to measure the fringes (relative time and phase offsets) between different sites. With the fringe solutions, the software correlator produced coherently added voltage data with an effective bandwidth of 112 MHz centred at 1388 MHz,[4] which were then processed with the DSPSR software (for details, see van Straten & Bailes 2011) to extract the single pulse data. The data were coherently dedispersed using a dispersion measure (DM) of 15.9891 cm^{-3} pc (which is the default value used at JBO to de-disperse PSR J1713+0747 data). Single pulse data were written to discs with a maximum time resolution of 140 ns (corresponding to 32 768 phase bins within a period). More details of our data processing pipeline are described in Bassa et al. (2016).

Fig. 1 shows the total intensity profile from the LEAP data compared with those from each of the single telescopes. A calculation based on S/N measurements shows a coherency of 95 per cent for the LEAP addition. The polarization profile as well as the swing of linear polarization position angle (P.A.) from the LEAP data shown in Fig. 2 is consistent with the results from previous work (Ord et al. 2004; Yan et al. 2011). We also used the receiver properties measured from PSR J1713+0747 to calibrate PSR J1600−3053 data obtained on the same epoch, and had consistent result as shown in the EPN data base.

The variability of single pulse emission is commonly investigated using a set of statistical tools. The modulation index is used to indicate the level of intensity variation. The fluctuation (power) spectra of pulse intensity as a function of pulse number and rotational phase (pulse stack) can identify periodicities in the emission. The longitude-resolved fluctuation spectrum (LRFS) resolves the fluctuations as a function of rotational phase. The two-dimensional fluctuation spectrum (2DFS) is calculated by performing a two-dimensional Fourier Transform of the pulse stack, which is widely used to study the systematic drifting of sub-pulses. Details of these statistical tools can be found in, for example, Edwards & Stappers (2003) and Weltevrede et al. (2006b). The software tools used to conduct single pulse analysis in this paper are part of the PSRSALSA project (Weltevrede 2016), and are freely available online.[5]

3 RESULTS

The observation recorded a total of 196 915 single pulses, approximately 75 per cent of which were detected with a peak S/N higher than 5 based on a time resolution of 9 μs. The highest peak S/N is 36, a factor of 3 greater than the maximum recorded in Shannon & Cordes (2012). Fig. 3 shows an example stack of 100 consecutive pulses, which shows clear intensity variation among the pulses. During the 15-min observation, the flux density of the pulsar dropped by approximately 10 per cent due to interstellar scintillation.

3.1 Single pulse properties

The energy distribution of single pulses from PSR J1713+0747 has been studied in previous work (Shannon & Cordes 2012; Shannon et al. 2014), based on either the peak flux density or the total flux density from a chosen on-pulse region. Here we used the single pulse data to study the energy distribution in three phase ranges that correspond to the leading edge, the peak, and the trailing edge of the integrated profile (see Fig. 4). The observed pulse energy was calculated by summing the intensities within the corresponding phase range defined in Table 1 after subtracting the off-pulse mean. The corresponding noise energy distributions were obtained from an equally long phase range in the off-pulse region. To compensate for

[3] http://www.epta.eu.org/epndb/

[4] Data from the 1452 MHz sub-band were not included due to a receiver cutoff at Effelsberg.

[5] https://github.com/weltevrede/psrsalsa

Downloaded from http://mnras.oxfordjournals.org/ at INAF Cagliari (Osservatorio Astronomico di Cagliari) on November 10, 2016

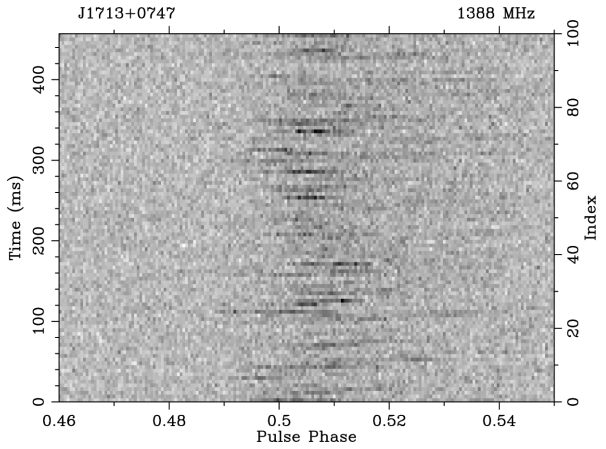

Figure 3. An example of a pulse stack containing 100 pulses. The time resolution used here is 2.3 μs. The figure illustrates the pulse-to-pulse variation which is analysed quantitatively further below (see Fig. 7).

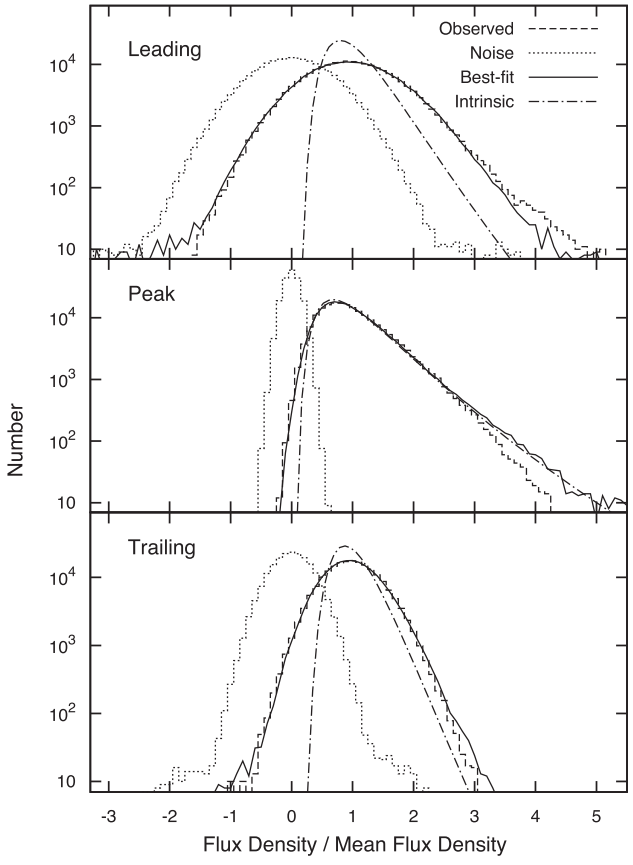

Figure 4. Pulse energy distributions in phase ranges (detailed in Table 1) corresponding to the leading edge, the peak, and the trailing edge of the integrated profile. The dashed, dotted, solid, and dash–dotted lines represent the observed pulse energy distribution, the noise energy distribution, the best fit to the observed distribution, and the modelled intrinsic pulse energy distribution with a log-normal function, respectively.

the variation in flux density caused by scintillation, the data were first re-scaled to ensure that the average pulse energy in subsequent 30-s intervals remains constant. The observed energy distribution was modelled by convolving an intrinsic distribution, here assumed to be log-normal, with the observed noise distribution via a procedure detailed in Weltevrede et al. (2006a) and Weltevrede (2016). The log-normal probability density function is defined as

$$\rho(x) = \frac{1}{\sqrt{2\pi}x\sigma}\exp\left[-\frac{(\ln x - \mu)^2}{2\sigma^2}\right]. \quad (1)$$

For each region, the observed and the modelled intrinsic pulse energy distributions are shown in Fig. 4. It can be seen that the three regions have a different intrinsic pulse energy distribution, that of the peak region being broadest. A Kolmogolov–Smirnov (KS) test (summarized in Table 1) shows that in all three cases the intrinsic pulse energy can be well described by an intrinsically log-normal distribution.

In Fig. 5, we plot the number density distribution of pulses with respect to their relative peak flux densities and phases of the pulse peak. We note that pulses with higher peak flux densities tend to be located within a narrow phase range that includes the maximum of the integrated profile. Lower-amplitude pulses can occur in a wider phase range which extends more to the trailing edge of the integrated profile. This confirms the finding in Shannon & Cordes (2012), and indicates that the phase distribution of these pulses is not symmetric. More investigations into the impact on timing follow in Section 3.3. The occurrence rate of bright pulses whose relative peak flux densities are larger than 3 was found to be constant during the observation.

It was shown in Liu et al. (2015) that the bright single pulses from the MSP J1022+1001 have a preferred pulse width for any given peak flux density. To investigate whether a similar feature is present in the pulses of PSR J1713+0747, in Fig. 6 we plotted the number

Table 1. Phase (see Fig. 1 to correspond to the integrated profile) ranges defined for the leading edge, the peak, and the trailing edge of the integrated profile, p-values from a KS test on the modelled and the observed pulse energy distributions in these three regions, and the best-fitting modelling parameters as defined in equation (1). None of these p-values indicates a significant difference between the modelled and observed distributions.

	Phase range	p-value	μ	σ
Leading	(0.400, 0.500)	0.99	−0.090	0.37
Peak	(0.500, 0.515)	0.60	−0.12	0.52
Trailing	(0.515, 0.615)	0.67	−0.052	0.30

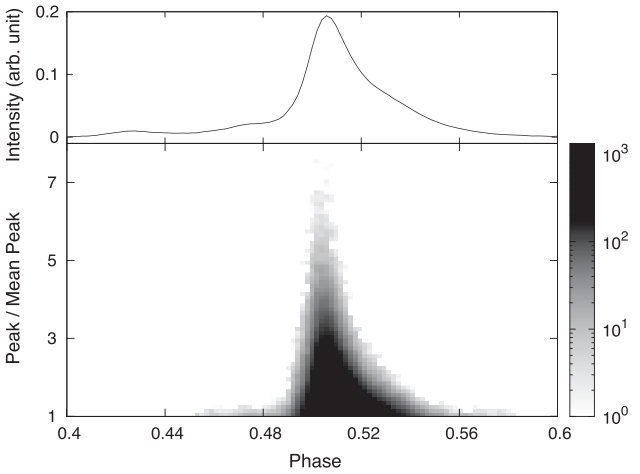

Figure 5. Number density distribution (lower panel) of pulses with respect to their relative peak flux densities and phase of pulse peak, compared with the integrated profile (upper panel). Here we used a time resolution of 9 μs for the data.

Downloaded from http://mnras.oxfordjournals.org/ at INAF Cagliari (Osservatorio Astronomico di Cagliari) on November 10, 2016

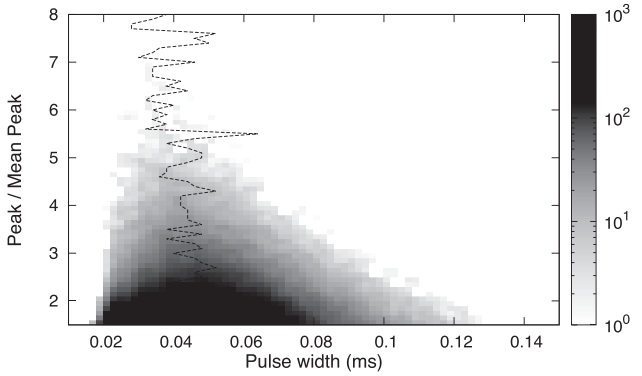

Figure 6. Number density distribution of pulses with respect to their relative peak flux density and width. The peak bins were selected based on a time resolution of 9 μs. The dashed line shows the pulse width corresponding to the maximum number density for a given peak flux density.

density distribution of pulses with respect to their relative peak flux density and width. Here we define pulse width as the full width at 50 per cent of the peak amplitude (i.e. W_{50}), as in, for example, Lyne et al. (2010). We found that a pulse width of roughly 0.04 ms is favoured for the bright single pulses, which is smaller than the W_{50} of the integrated profile (0.11 ms).

To investigate the variability of single pulses, we have calculated the longitude-resolved modulation index, the LRFS, and the 2DFS based on the entire length of the observation (Fig. 7). Here, we used the same definitions as in Weltevrede et al. (2006b). The modulation index as a function of pulse phase was found to be consistent with the results in Edwards & Stappers (2003) and Shannon & Cordes (2012), and yields a significantly improved resolution. It is maximized at the extreme edges of the integrated profile, which is commonly seen in canonical pulsars (e.g. Weltevrede et al. 2006b). The asymmetric distribution of the modulation index also indicates that the intensity variation is different in the leading and trailing edges of the integrated profile, as expected from the results in Fig. 4. In the LRFS shown in Fig. 7, two maxima are visible at 0.14 and 0.34 cpp. This detection confirms the discovery of periodic intensity modulation by Edwards & Stappers (2003) with much higher significance. For better visualization of the two modes of periodicity, we subtracted the mean power in each spectrum (i.e. column) and plotted the modified LRFS in Fig. 8. It can be seen that both periodicities occur at the phase of the main peak of the integrated profile. The mode with periodicity of 0.14 cpp extends further to the trailing edge of the integrated profile, where no significant power was detected corresponding to the periodicity of 0.34 cpp. While similar phenomena are known to occur in canonical pulsars (e.g. Kramer, Johnston & van Straten 2002), this is the first time a phase-dependent periodicity of intensity variations has been reported for a MSP.

In the 2DFS, the two local maxima at 0.14 and 0.34 cpp are clearly offset from the vertical axis of zero, indicating the association of the two periodicities with systematic drifting of emission power in pulse phase. Following the description in Weltevrede et al. (2006b), we have measured the horizontal separation of the drifting in pulse longitude (P_2) and their vertical separation in pulse periods (P_3) for the two modes, which are (15^{+2}_{-6} deg, $6.9 \pm 0.1\ P$) and (23^{+2}_{-14} deg, $2.9 \pm 0.1P$), respectively. Here P denotes the rotational period of the pulsar. Both modes show power over a broad range of P_3, meaning that the intensity variation does not follow one constant periodicity. The discovery of two drifting modes together with their overlap

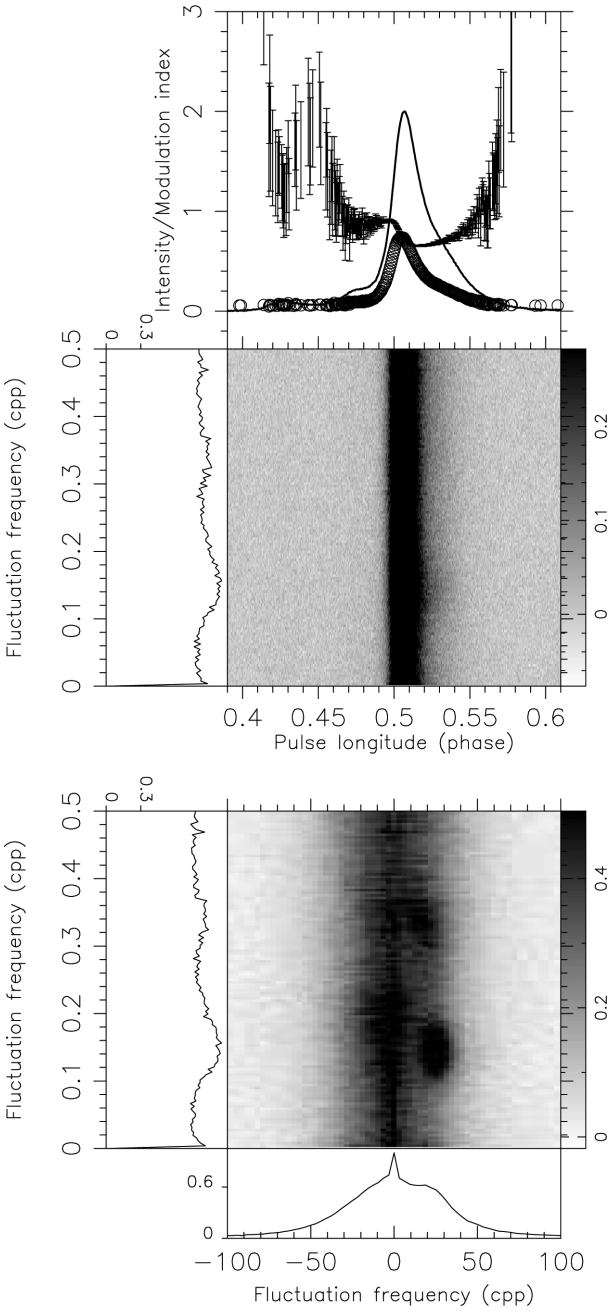

Figure 7. Statistical results from analysing the pulse stack from the entire 15-min observation. The top panel shows the integrated profile (solid line), longitude-resolved modulation index (points with error bars), and longitude-resolved standard deviation (open circles). The LRFS is plotted below this panel. Below the LRFS, the 2DFS is shown and the power in the 2DFS is vertically integrated and then normalized with respect to the peak value to produce the bottom plot. Both the LRFS and 2DFS are horizontally integrated and then normalized with respect to the peak value to produce the left side-panels of the spectra. The right side-panels label the colour scale (in arbitrary unit) in the LRFS and 2DFS, respectively.

in pulse phase suggests that either the two modes appear at the same time at the same rotational phase, or that the modes alternate. Following the description in Serylak, Stappers & Weltevrede (2009), a potential mode switch corresponding to the two periodicities was searched for by calculating the time-resolved 2DFS with a resolution from 10 to 50 pulses. The brightest part of the observation was

Downloaded from http://mnras.oxfordjournals.org/ at INAF Cagliari (Osservatorio Astronomico di Cagliari) on November 10, 2016

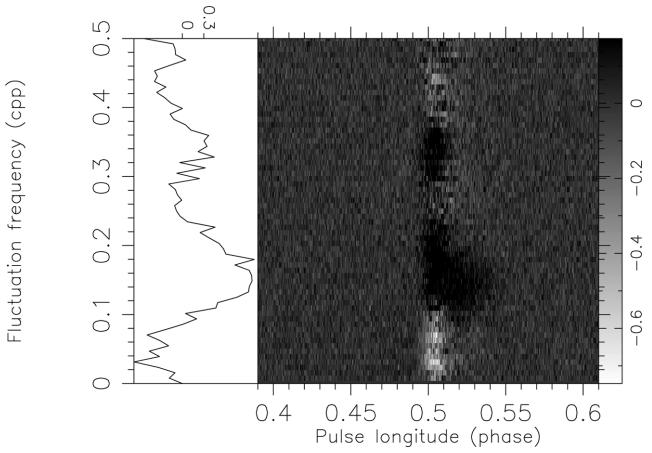

Figure 8. The same LRFS as in Fig. 7, but with the mean power subtracted in each column. The spectrum is horizontally integrated and then normalized with respect to the peak value, producing the side panel. The right side-panel label the colour scale in the LRFS with power in arbitrary unit.

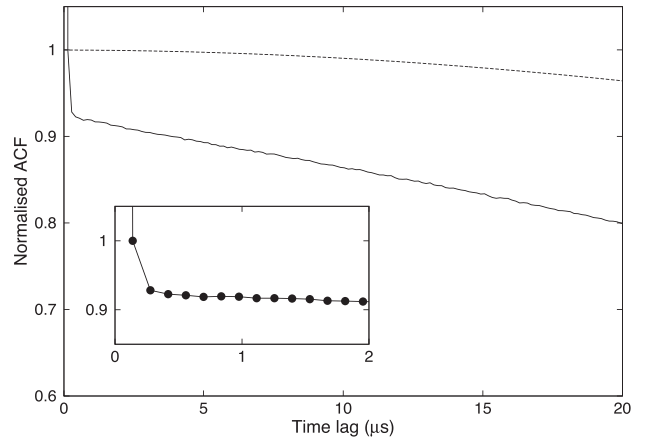

Figure 9. Averaged ACF of all single pulses (solid line) compared with the ACF of the averaged profile (dashed line). The inner panel shows a zoomed version of the plot in the 0–2 μs range. Here, we retained the highest time resolution of 140 ns for the profiles.

examined, but our sensitivity was insufficient to confirm if any transitions occurred on these short time-scales.

Previous high-time resolution observations have shown that periodic micro-structure in pulse emission is common for canonical pulsars (Cordes 1979). The duration of each micropulse can range from several hundreds down to several microseconds (Craft, Comella & Drake 1968; Bartel & Sieber 1978). However, no such phenomenon has thus far been found in MSPs (e.g. Jenet et al. 1998). To search for periodic micro-structure in PSR J1713+0747, following the definition in Lange et al. (1998), we calculated the averaged autocorrelation function (ACF) over all single pulses compared with the ACF of the averaged profile in Fig. 9. The highest time resolution of 140 ns in the data was retained to optimise the sensitivity to narrow features. Here, because the zero-lag bin of the averaged ACF from single pulses has a power exceeding 20 times of the other bins, we used the power in the first non-zero-lag bin to normalize the ACF in both cases. The comparison between the ACFs suggests that the single pulses are significantly narrower than the averaged profile. The slope of the averaged ACF over all single pulses changes at around 280 ns (the second non-zero-lag bin). Similar behaviour in the same type of ACF has already been witnessed in canonical pulsars (Hankins 1972; Lange et al. 1998). However, here we cannot rule out the cause by instrumental effect as the change of slope was also seen in the ACF calculated based on the off-pulse region. No reappearing local maximum has been seen from either ACF, ruling out the presence of periodic micro-structure. We further examined the ACFs of the brightest 100 single pulses, based on both peak flux density and total flux density, and again found no evidence of micro-structure. In order to rule out potential DM smearing that may lead to the non-detection, we refolded the brightest 10 pulses with different DMs ranging from 15.9879 to 15.9983 cm^{-3} pc,[6] in increments of 4×10^{-4} which corresponds to 120 ns smearing time for our observing frequency and bandwidth. The ACFs again showed no sign of micro-structure.

3.2 Single pulse polarization

The polarization properties of single pulses from MSPs have not been widely investigated by previous studies due to both the lack of sensitivity and hardware constraints. With the coherently added voltage data as recorded by LEAP, it was possible to retain full polarization information for all single pulses with proper calibration. Example polarization profiles can be found in Fig. 10, where we show the nine highest S/N pulses. We found that all these pulses show significant linear polarization, whose fraction with respect to the total intensity appears to be higher when compared with the integrated profile (Fig. 2). This indicates that the polarization fraction may depend on the brightness of the pulses. For further investigation, in Fig. 11 we grouped the single pulses based on their peak flux density and calculated the polarization fractions from their averages. The bias in linear and circular polarization was corrected following Simmons & Stewart (1985) and Tiburzi et al. (2013). The rise of polarization fraction for both L and V with increasing peak flux density is clearly shown. Note that similar dependence has already been seen in a handful of canonical pulsars and another MSP (Mitra, Gil & Melikidze 2009; Osłowski et al. 2014), while an opposite dependence was also noticed in one case (Xilouris et al. 1994).

The P.A. curve of the integrated profile in Fig. 2 shows a few discontinuities of approximately 90° difference, which usually indicates the existence of orthogonal polarization modes (OPMs). Following Gil & Lyne (1995) and Osłowski et al. (2014), in Fig. 12 we calculated the probability density distribution of P.A. measured from single pulse data, and compared with the P.A. swing obtained from the integrated profile (Fig. 2). Here, we only used samples with a corresponding linear intensity exceeding 3σ of detection. For a given phase, we formed the number density distribution with each count weighted by the inverse of its measurement variance, and normalized the distribution by its sum. The P.A. values of the single pulses between phase 0.494 and 0.530 (mode 2) were found to be rotated by 90° compared to adjacent phase ranges (mode 1), which corresponds to the two jumps in the P.A. curve of the integrated profile. Both the P.A. swing in the integrated profile and the P.A. distribution of the single pulses show a rapid change around phase 0.6. However, the low degree of linear polarization makes it impossible to distinguish between a smooth transition and a discontinuity. In either case the P.A. changes by less than 90°.

[6] The central value of the range is 15.9935 cm^{-3} pc, the DM on the observation epoch derived from Desvignes et al. (2016). The chosen range also covers the default DM value used in dedispersing the data.

Downloaded from http://mnras.oxfordjournals.org/ at INAF Cagliari (Osservatorio Astronomico di Cagliari) on November 10, 2016

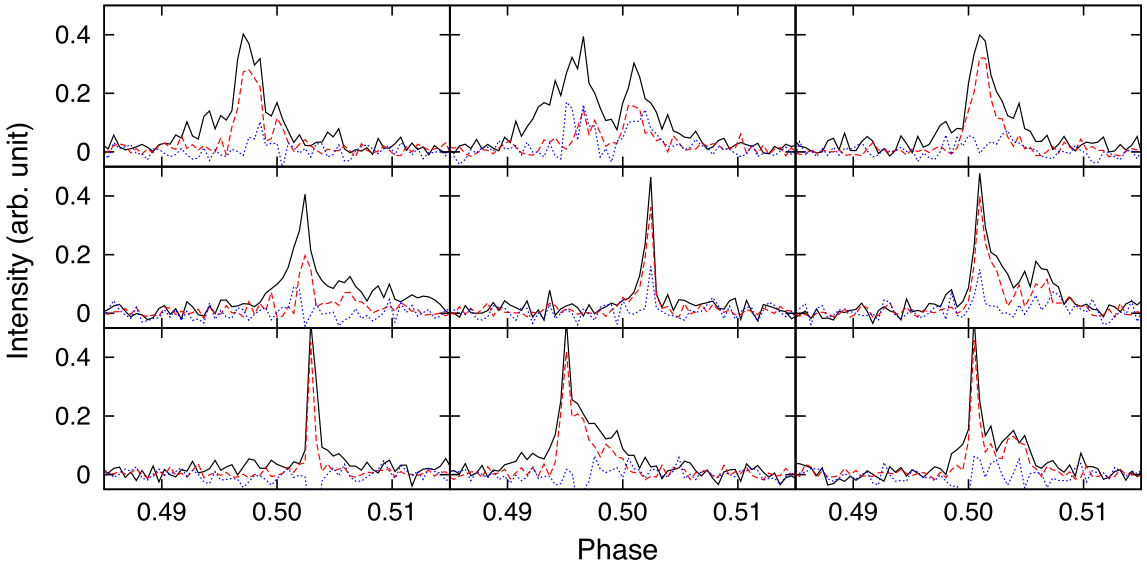

Figure 10. Polarization profiles of the nine highest-S/N pulses. The definition of the lines is the same as in Fig. 2. The time resolution in this plot is 2.3 μs.

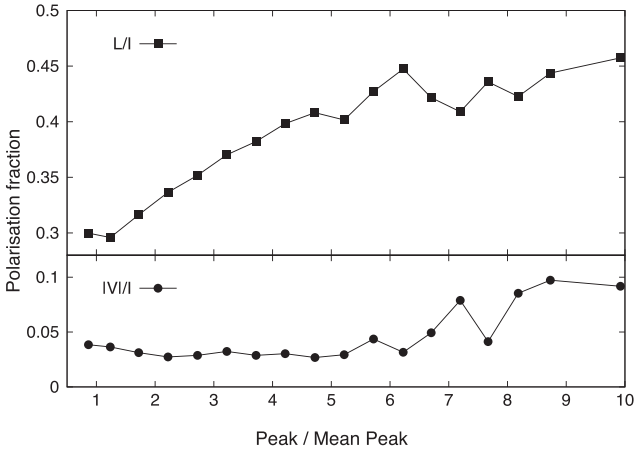

Figure 11. Polarization fractions of linear (top) and circular (bottom) component, as a function of relative peak flux density of single pulses.

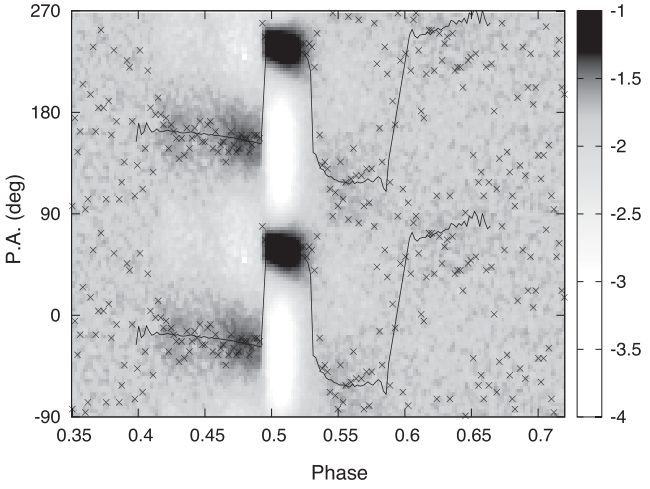

Figure 12. Longitude-resolved probability density distribution of P.A. values from single pulses in log-scale. The values were selected if the corresponding linear polarization exceeds 3-σ. The crosses represent the maximum of probability for each phase bin. The solid line shows the P.A. curve from the integrated profile. Note that between phase 0.59 and 0.60 there is no available P.A measurement due to the lack of sufficient linear intensity. All P.A. values were plotted twice (with 360° separation) for clarity.

Within some ranges of pulse phase, in particular those corresponding to mode 1, the most-likely value of P.A. is widely scattered, covering a range of nearly 90°. For several selected phase bins, we checked the number density distributions of P.A. which turned out to be spread over at least a few tens of degrees, broader than what is expected purely from instrumental noise (less than 10°). The widths of the distributions grow as the linear intensity decreases. Such phenomena have already been noticed in many canonical pulsars (e.g. Stinebring et al. 1984; McKinnon & Stinebring 1998; Karastergiou et al. 2002). To examine if the distribution of P.A. are different in the two modes, we chose pulse phases of the same linear intensity in the integrated profile, and plotted the distribution of P.A. values with measurement error less than 7°.[7] The result is shown in Fig. 13, where the distribution from mode 1 is seen to be broader than in mode 2. This also indicates the existence of an intrinsic P.A. distribution instead of a single value. A recovery of the intrinsic distribution, however, would require a detailed modelling of the instrumental noise which additionally takes into account the covariance of the noise component in the measured Stokes Q and U (van Straten 2010).

[7] The measurement uncertainties were obtained by standard error propagation using the variance of Stokes Q and U. It is expected to give the 1-σ error, when the S/N of the linear intensity exceeds 3 which corresponds to an error of approximately 9°.6 in P.A. (Wardle & Kronberg 1974).

3.3 Impact on timing

The variability of single pulses introduces a variation in the integrated profile. This manifests itself as stochastic fluctuations in the derived pulse time-of-arrivals (TOAs), which is commonly known as phase jitter. Shannon & Cordes (2012) have shown that the timing precision of PSR J1713+0747 on short time-scales can be greatly limited by phase jitter. The subsequent jitter noise in the timing data scales as the square-root of number of averaged pulses, as expected

Downloaded from http://mnras.oxfordjournals.org/ at INAF Cagliari (Osservatorio Astronomico di Cagliari) on November 10, 2016

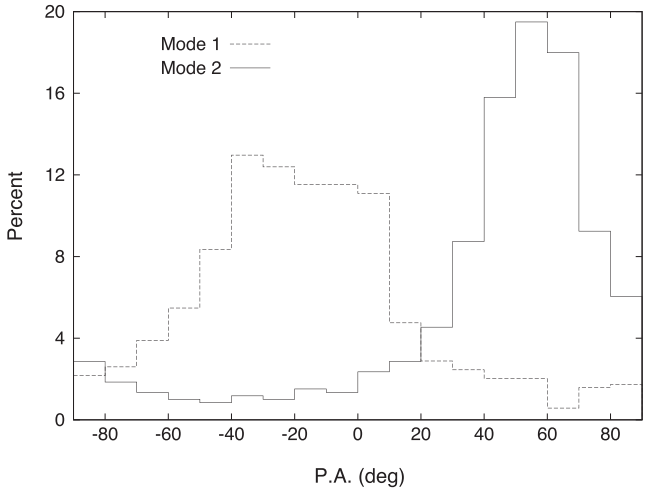

Figure 13. Number densities of P.A. (normalized by the sum) from pulse phase 0.475 (dashed line) and 0.522 (solid line), which correspond to different OPMs. The linear intensities in the integrated profile are the same at the two phases.

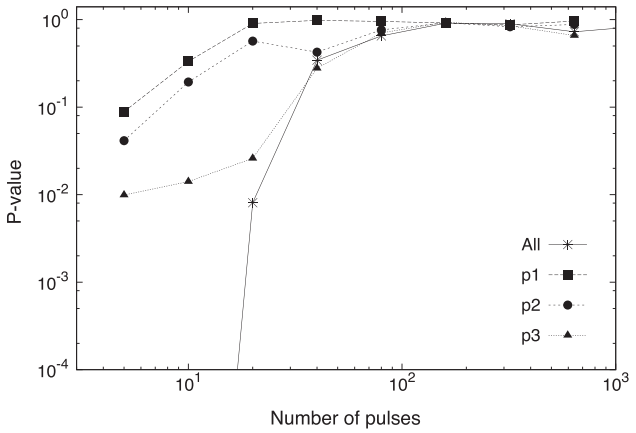

Figure 14. Measured p-values from standard KS test of weighted timing residuals based on different numbers of averaged pulses, obtained from all pulses as well as sub-sets of pulses based on their peak flux densities. Details of the three sub-sets can be found in Table 2.

from the theoretical model (e.g. Cordes & Downs 1985). Following the method described in Liu et al. (2012), we measured jitter noise of 494 ns in our data for a 10-s integration time, in agreement with the finding in Shannon & Cordes (2012). Consistent results were also found when we made the measurements with data from each 16-MHz sub-band instead of using the full bandwidth.

The phase jitter of integrated profiles is usually assumed to follow a Gaussian distribution. However, if single pulses are not normally distributed in rotational phase, the resulting jitter noise is likely to deviate from Gaussian noise, especially when the number of averaged pulses is not sufficiently large. For PSR J1713+0747, the asymmetric occurrence rate of single pulses in rotational phase is clear from Fig. 5, which was also shown in Shannon & Cordes (2012). To further investigate the nature of the jitter noise, we produced timing residuals based on different numbers of averaged pulses, weighted them by the sum of radiometer and jitter noise, and calculated their p-values[8] from a standard KS test under the hypothesis of a normal distribution (Fig. 14). We can see that the phase jitter starts to appear as Gaussian noise only after integrating $\sim 10^2$ pulses. Integrating a sub-set of pulses selected based on a chosen range of peak flux densities gives a relatively quick conversion, as expected. This places a lower limit on the number of pulses (i.e. $\sim 10^2$) to be integrated in timing analysis to avoid significant non-Gaussianity. Note that a similar limit was already derived for PSR J0437−4715, based on simulations of the regularity of profile shapes (Liu et al. 2011).

Single pulses do not necessarily have the same variability as a function of rotational phase (e.g. Cognard et al. 1996; Liu et al. 2015), meaning that their contribution to the resulting jitter noise can be different. In Osłowski et al. (2014), single pulses from PSR J0437−4715 were grouped based on their peak flux density and averaged into integrated profiles, which did not result in a significant improvement of the timing precision. Following this, we divided the pulses into groups based on their relative peak flux densities, relative total flux densities and widths, separately. Subsequently, we produced timing residuals containing the same number of TOAs from each group.[9] The results are summarized in Table 2. It can be seen that all sub-sets contribute approximately the same jitter noise per pulse, though pulses of high flux density and narrow width tend to show slightly lower values. The achieved timing rms values are also significantly higher than when using all pulses. Thus, there is no apparent benefit in grouping the single pulses for the purpose of precision timing.

Table 2. Timing residuals achieved with different sub-sets of pulses. The pulses are grouped with respect to their relative peak flux density (p, peak flux density divided by its running mean), relative flux density (f, total flux density divided by its running mean) and pulse width (w, defined as W_{50}). The rms values are calculated based on the same number of TOAs.

	Range	Per cent	rms (μs)	$\chi^2_{\rm re}$	$\sigma_{\rm j,\,0}$ (μs)
$p1$	(0, 1.17)	35.4	1.01	2.75	22.5
$p2$	(1.17, 1.60)	31.3	1.02	8.20	25.1
$p3$	(1.60, 3.00)	29.3	0.816	18.9	20.2
$p4$	(3.00, +∞)	3.93	1.97	69.4	18.3
$f1$	(0, 0.77)	31.7	1.04	2.87	22.1
$f2$	(0.77, 1.05)	26.6	1.11	9.98	25.4
$f3$	(1.05, 1.39)	25.7	0.862	10.5	19.5
$f4$	(1.39, +∞)	16.0	0.935	18.5	17.1
$w1$	(0, 30) μs	33.9	1.06	3.70	21.1
$w2$	(30, 50) μs	35.5	0.833	11.3	21.2
$w3$	(50, +∞) μs	30.6	0.867	17.8	21.2
All	(0, +∞)	100	0.590	12.9	26.5

In principle, the achievable TOA precision should be independent of the choice of time resolution ($\delta\tau$) in forming the integrated profile, as far as its features are fully resolved (e.g. Downs & Reichley 1983). Here, we used the single pulse data to form integrated profiles of 1-s integrations and variable time resolution, and calculated their corresponding TOA uncertainties. On average, the TOA uncertainty drops no more than 5 per cent when $\delta\tau$ decreases

[8] Such a p-value close to unity shows that we cannot detect significant deviation from the normal distribution of data.

[9] The TOAs were estimated with the standard template matching algorithm (Taylor 1992). To time each sub-set of pulses, we formed the template by integrating the whole sub-set and performed wavelet-smoothing to the integrated profile, to avoid self-correlation by the noise. The residuals were calculated with the ephemeris from Desvignes et al. (2016), without any fit for the timing parameters.

Downloaded from http://mnras.oxfordjournals.org/ at INAF Cagliari (Osservatorio Astronomico di Cagliari) on November 10, 2016

from 8.9 μs to 140 ns. This suggests that the narrow features in the single pulses are mostly averaged out, and a time resolution beyond 10 μs is sufficient in shaping the profiles when the exposure time is longer than one second.

4 CONCLUSIONS AND DISCUSSIONS

We have studied the properties of single pulses from PSR J1713+0747 using 15 min of data (corresponding to ∼197 000 pulses) collected by LEAP when the pulsar was extremely bright. The pulse energy distribution is shown to be consistent with a log-normal distribution. The pulse widths are typically around 0.04 ms for the bright pulses. In addition, we have confirmed the detection of periodic intensity modulation by Edwards & Stappers (2003), and in addition revealed its association with systematic drifting sub-pulses. From the 2DFS, P_2 and P_3 of the two modes were measured to be (15^{+2}_{-6} deg, 6.9 ± 0.1P) and (23^{+2}_{-14} deg, 2.9 ± 0.1P), respectively. The occurrence of the two modes is found to overlap at the phase of the main peak in the integrated profile, providing the first evidence for superposed modes of drifting sub-pulse in MSPs. The mode at 0.14 cpp was also apparent at the trailing edge of the integrated profile, where the other was not detected. We did not find any evidence of periodic pulse micro-structure with a time resolution of up to 140 ns. With full polarization data, we have shown that the bright pulses are significantly linearly polarized. On average, the fractional polarization of the pulses increases with increasing pulse peak flux density. Using single pulse polarization, we have presented a longitude-resolved probability density map of P.A., and shown the existence of two orthogonal modes of polarization that are clearly distinct in pulse phase. Finally, we found that jitter noise induced by pulse variability can be described as Gaussian only when at least 100 pulses have been integrated. Statistically, pulses of different properties contribute equally to the resulting jitter noise, though pulses with high peak flux density have slightly less effect. By timing sub-sets of pulses with respect to their relative peak flux density, relative total flux density and pulse width, we did not find any significant improvement in the overall timing precision. Changing the time resolution used on 1-s integrations from 8.9 μs to 140 ns does not result in significant difference in their TOA uncertainties, meaning that most features on those integrated profiles are resolved with time resolution beyond 10 μs.

Micro-structure in pulsed radio emission has mostly been searched for in canonical pulsars, and most of the searches that have sufficient time resolution and sensitivity have achieved successful detection (e.g. Lange et al. 1998; Mitra, Arjunwadkar & Rankin 2015). On the other hand, besides PSR J1713+0747, micro-structure has also been searched for in another two MSPs, PSR J0437−4715 and PSR B1937+21, with no detection (Jenet et al. 1998; Jenet et al. 2001). Using observations of canonical pulsars, Kramer et al. (2002) established a relation between micro-structure width and pulsar rotational period. A simple extrapolation from that relation leads to a micro-structure width of 0.5–10 μs for MSPs, well above the time resolutions of the data used for the searches in MSPs. Thus, the non-detections may imply that either micro-structure is less common in MSPs compared with the situation in canonical pulsars, or the relation between micro-structure width and rotational period is different in MSPs. Nevertheless, this needs to be further verified by more sample studies.

The discovery of drifting sub-pulses in PSR J1713+0747 increases the number of MSP 'drifters' to three, together with PSR J1012+5307 and J1518+4904 (Edwards & Stappers 2003). As high-sensitivity searches for drifting sub-pulses have been performed in no more than 10 MSPs, drifting sub-pulses do not seem to be an unusual phenomenon among this part of the pulsar population. It is interesting to note that all three exhibit a quasi-periodic drifting fashion, and are classified as 'diffuse' drifter by the definition in Weltevrede et al. (2006b). Given that nearly half of the drifters in canonical pulsars show a precise drifting period (referred to as 'coherent' drifters), quasi-periodic drifting may be comparatively more common in MSPs. Again, robust statistics of the ratio requires future work including an expanded number of samples. Searching for drifting sub-pulses in more MSPs will also show if the phenomenon is correlated with any pulsar properties, such as the characteristic age which has been discovered among the population of non-recycled pulsars (Weltevrede et al. 2006b; Weltevrede, Stappers & Edwards 2007).

Despite the vast increase in sensitivity delivered by LEAP, a thorough understanding of single pulse properties, in particular those from the lower end of the energy distribution, is still limited by S/N. The situation is likely to be significantly improved when coherent addition of the pulse signal is achieved with more telescopes, as also suggested in Dolch et al. (2014). Eventually, the next generation of radio telescopes, e.g. the Square Kilometre Array and the Five hundred metre Aperture Spherical Telescope, will provide the best opportunity ever to study single pulse emission from MSPs.

The behaviour of pulse variability is seen to be a source-dependent phenomenon among pulsars including MSPs. Despite the lack of improvement in the timing precision of PSR J1713+0747, single pulse data could still be used to mitigate jitter noise in some other pulsars, especially when pulses with different properties exhibit different distributions in phase. In this case, a weighting scheme concerning their contribution to jitter noise may be introduced when integrating the pulses, so as to optimally use the signal of the pulses which show less variability in phase. An approach in a similar framework has already been discussed in Imgrund et al. (2015). Nevertheless, implementation of such methods is yet to be thoroughly investigated.

ACKNOWLEDGEMENTS

We would like to thank S. Osłowski, A. Noutsos and J. M. Cordes for valuable discussions, I. Cognard for assistance in observations at Nançay, and A. Jessner for carefully reading the manuscript and providing valuable insights. We also thank the anonymous referee for providing constructive suggestions to improve the article. KL acknowledges the financial support by the European Research Council for the ERC Synergy Grant BlackHoleCam under contract no. 610058. This work is supported by the ERC Advanced Grant 'LEAP', Grant Agreement Number 227947 (PI M. Kramer). The Effelsberg 100-m telescope is operated by the Max-Planck-Institut für Radioastronomie. The Westerbork Synthesis Radio Telescope is operated by the Netherlands Foundation for Radio Astronomy, ASTRON, with support from NWO. The Nançay Radio Observatory is operated by the Paris Observatory, associated with the French Centre National de la Recherche Scientifique. CGB and SS acknowledge support from the European Research Council under the European Union's Seventh Framework Programme (FP/2007-2013) / ERC Grant Agreement nr. 337062 (DRAGNET; PI Jason Hessels). RS acknowledges the financial support from the European Research Council under the European Union's Seventh Framework Programme (FP/2007-2013)/ERC Grant Agreement n. 617199. KJL gratefully acknowledges support from National Basic Research Program of China, 973 Program, 2015CB857101 and NSFC U15311243. This research is a result of the common effect to

Downloaded from http://mnras.oxfordjournals.org/ at INAF Cagliari (Osservatorio Astronomico di Cagliari) on November 10, 2016

directly detect gravitational waves using pulsar timing, known as the European Pulsar Timing Array (EPTA).

REFERENCES

Alpar M. A., Cheng A. F., Ruderman M. A., Shaham J., 1982, Nature, 300, 728
Antoniadis J. et al., 2013, Science, 340, 448
Arzoumanian Z. et al., 2015, ApJ, 813, 65
Arzoumanian Z. et al., 2016, ApJ, 821, 13
Bartel N., Sieber W., 1978, A&A, 70, 260
Bassa C. G. et al., 2016, MNRAS, 456, 2196
Bilous A. V., 2012, PhD thesis, University of Virginia
Bilous A. V., Pennucci T. T., Demorest P., Ransom S. M., 2015, ApJ, 803, 83
Caballero R. N. et al., 2016, MNRAS, 457, 4421
Cairns I. H., Johnston S., Das P., 2004, MNRAS, 353, 270
Cheng A. F., Ruderman M., 1977, ApJ, 212, 800
Cognard I., Shrauner J. A., Taylor J. H., Thorsett S. E., 1996, ApJ, 457, L81
Cordes J. M., 1976, ApJ, 210, 780
Cordes J. M., 1979, Space Sci. Rev., 24, 567
Cordes J. M., Downs G. S., 1985, ApJS, 59, 343
Craft H. D., Comella J. M., Drake F., 1968, Nature, 218, 1122
Demorest P. B., Pennucci T., Ransom S. M., Roberts M. S. E., Hessels J. W. T., 2010, Nature, 467, 1081
Desvignes G., Barott W. C., Cognard I., Lespagnol P., Theureau G., 2011, in Burgay M., D'Amico N., Esposito P., Pellizzoni A., Possenti A., eds, AIP Conf. Ser. Vol. 1357, RADIO PULSARS: AN ASTROPHYSICAL KEY TO UNLOCK THE SECRETS OF THE UNIVERSE. Am. Inst. Phys., New York, p. 349
Desvignes G. et al., 2016, MNRAS, 458, 3341
Dolch T. et al., 2014, ApJ, 794, 21
Downs G. S., Reichley P. E., 1983, ApJS, 53, 169
Drake F. D., Craft H. D., 1968, Nature, 220, 231
Edwards R. T., Stappers B. W., 2003, A&A, 407, 273
Edwards R. T., Stappers B. W., 2004, A&A, 421, 681
Freire P. C. C. et al., 2012, MNRAS, 423, 3328
Gil J., 1985, ApJS, 110, 293
Gil J. A., Lyne A. G., 1995, MNRAS, 276, L55
Gil J., Melikidze G. I., Geppert U., 2003, A&A, 407, 315
Hankins T. H., 1972, ApJ, 177, L11
Imgrund M., Champion D. J., Kramer M., Lesch H., 2015, MNRAS, 449, 4162
Janssen G. et al., 2015, Proc. Sci., Gravitational Wave Astronomy with the SKA. SISSA, Trieste. PoS#037
Jenet F., Anderson S., Kaspi V., Prince T., Unwin S., 1998, ApJ, 498, 365
Jenet F. A., Anderson S. B., Prince T. A., 2001, ApJ, 546, 394
Karastergiou A., Kramer M., Johnston S., Lyne A. G., Bhat N. D. R., Gupta Y., 2002, A&A, 391, 247
Karuppusamy R., Stappers B., van Straten W., 2008, PASP, 120, 191
Knight H. S., 2007, MNRAS, 378, 723
Knight H. S., Bailes M., Manchester R. N., Ord S. M., Jacoby B. A., 2006, ApJ, 640, 941
Kramer M., Johnston S., van Straten W., 2002, MNRAS, 334, 523
Kramer M. et al., 2006, Science, 314, 97
Lange C., Kramer M., Wielebinski R., Jessner A., 1998, A&A, 332, 111
Lazarus P., Karuppusamy R., Graikou E., Caballero R. N., Champion D. J., Lee K. J., Verbiest J. P. W., Kramer M., 2016, MNRAS, 458, 868
Lentati L., Shannon R. M., 2015, MNRAS, 454, 1058
Lentati L. et al., 2015, MNRAS, 453, 2576
Liu K., Verbiest J. P. W., Kramer M., Stappers B. W., van Straten W., Cordes J. M., 2011, MNRAS, 417, 2916
Liu K., Keane E. F., Lee K. J., Kramer M., Cordes J. M., Purver M. B., 2012, MNRAS, 420, 361
Liu K. et al., 2015, MNRAS, 449, 1158
Lyne A. G., Graham-Smith F., 2006, Pulsar Astronomy. Cambridge Univ. Press, Cambridge
Lyne A., Hobbs G., Kramer M., Stairs I., Stappers B., 2010, Science, 329, 408
McKinnon M., Stinebring D., 1998, ApJ, 502, 883
Mitra D., Gil J., Melikidze G. I., 2009, ApJ, 696, L141
Mitra D., Arjunwadkar M., Rankin J. M., 2015, ApJ, 806, 236
Ord S. M., van Straten W., Hotan A. W., Bailes M., 2004, MNRAS, 352, 804
Osłowski S., van Straten W., Hobbs G. B., Bailes M., Demorest P., 2011, MNRAS, 418, 1258
Osłowski S., van Straten W., Bailes M., Jameson A., Hobbs G., 2014, MNRAS, 441, 3148
Özel F., Psaltis D., Ransom S., Demorest P., Alford M., 2010, ApJ, 724, L199
Qiao G. J., Lee K. J., Zhang B., Xu R. X., Wang H. G., 2004, ApJ, 616, L127
Rankin J. M., 1986, ApJ, 301, 901
Reardon D. J. et al., 2016, MNRAS, 455, 1751
Ruderman M. A., Sutherland P. G., 1975, ApJ, 196, 51
Serylak M., Stappers B. W., Weltevrede P., 2009, A&A, 506, 865
Shannon R. M., Cordes J. M., 2012, ApJ, 761, 64
Shannon R. M. et al., 2014, MNRAS, 443, 1463
Shannon R. M. et al., 2015, Science, 349, 1522
Simmons J. F. L., Stewart B. G., 1985, A&A, 142, 100
Smits R. et al., 2016, Astron. Comput., in press
Stairs I. H., Thorsett S. E., Camilo F., 1999, ApJS, 123, 627
Stinebring D. R., Cordes J. M., Rankin J. M., Weisberg J. M., Boriakoff V., 1984, ApJS, 55, 247
Taylor J. H., 1992, Phil. Trans. R. Soc. A, 341, 117
Tiburzi C. et al., 2013, MNRAS, 436, 3557
van Straten W., 2004, ApJ, 152, 129
van Straten W., 2010, ApJ, 719, 985
van Straten W., Bailes M., 2011, Proc. Astron. Soc. Aust., 28, 1
Verbiest J. P. W. et al., 2016, MNRAS, 458, 1267
Wardle J., Kronberg P., 1974, ApJ, 194, 249
Weisberg J. M., Nice D. J., Taylor J. H., 2010, ApJ, 722, 1030
Weltevrede P., 2016, A&A, 590, A109
Weltevrede P., Wright G. A. E., Stappers B. W., Rankin J. M., 2006a, A&A, 458, 269
Weltevrede P., Edwards R. T., Stappers B. W., 2006b, A&A, 445, 243
Weltevrede P., Stappers B. W., Edwards R. T., 2007, A&A, 469, 607
Xilouris K. M., Kramer M., Jessner A., Wielebinski R., 1994, A&A, 288, L17
Yan W. M. et al., 2011, MNRAS, 414, 2087
Zhu W. W. et al., 2015, ApJ, 809, 41
Zhuravlev V. I., Popov M. V., Soglasnov V. A., Kondrat'ev V. I., Kovalev Y. Y., Bartel N., Ghigo F., 2013, MNRAS, 430, 2815

This paper has been typeset from a TEX/LATEX file prepared by the author.

Downloaded from http://mnras.oxfordjournals.org/ at INAF Cagliari (Osservatorio Astronomico di Cagliari) on November 10, 2016